Langmuir

Article

pubs.acs.org/Langmuir

Characterization of Solid-Supported Dipalmitoylphosphatidylcholine Membranes Containing Cholesterol

James Kurniawan and Tonya L. Kuhl*

Department of Chemical Engineering and Materials Science, University of California, Davis, One Shields Avenue, Davis, California 95616, United States

Supporting Information

ABSTRACT: The incorporation of cholesterol into dipalmitoylphosphatidylcholine (DPPC) membranes, even in small amounts, has been shown to significantly alter the properties of the membrane. In this work, force−distance interaction profiles of DPPC membranes containing 8 mol % cholesterol obtained using the surface force apparatus are analyzed in the context of high-resolution structural characterization by atomic force microscopy and neutron reflectometry. The adhesion between the mixed membranes was greater than that for pure DPPC and was variable—depending on the number of defects in the outer membrane leaflets. These defects were only detectable by atomic force microscopy and had an average size of 230 ± 30 nm and 1−5% surface density in the outer leaflet. The adhesion between the membranes monotonically increased as the thickness of the membrane decreased—in direct correlation with the number of defects present (exposed hydrophobic groups) in the membrane contact region. Because of the low diffusion rate of gel-phase membranes, the interaction force profiles were stable and no membrane restructuring was observed.

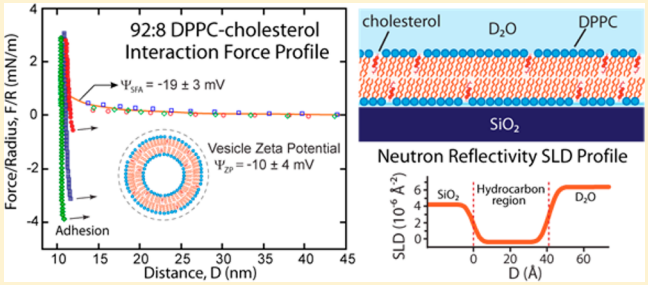

INTRODUCTION

Cholesterol is an important building block in biological membranes and is found in every cell in the human body. Cholesterol's ubiquitousness underlines its important role in altering the physical[1,2] and thermodynamic properties of membranes by changing the packing or the ordering of lipids, by reducing membrane permeability,[3−5] and in forming lipid rafts.[6−10] In particular, cholesterol is known to have a condensing effect on fluid-phase lipids and to conversely fluidize solid-phase lipids which helps maintain the integrity of cell membranes when stressed.[11,12] The concentration of cholesterol varies between different cell types and organelles with concentrations ranging from 5%[13] to as high as 50%[14] of the membrane. A plethora of studies have looked at the function of cholesterol in cell membranes and the effect of the addition of cholesterol in altering the intermolecular interactions in biomimetic membrane systems.[3,15−17] For example, phase diagrams of binary and ternary lipid mixtures containing cholesterol are well-documented,[18−20] and studies have also looked at the alteration of membrane mechanical properties due to preferential segregation of cholesterol.[2,8] In terms of high-resolution structural characterization, Mills et al.[21] quantified changes in the lamellar repeat distance in multilamellar dipalmitoylphosphatidylcholine (DPPC) vesicles with cholesterol using wide-angle X-ray scattering. They found that, in general, addition of cholesterol resulted in the tighter packing of DPPC lipids which induced an increase in membrane thickness and lamellar spacing. Further, 8 mol % cholesterol had the largest effect on altering the packing of DPPC as the mixture remains in the gel phase. Higher cholesterol concentrations result in coexisting gel and liquid ordered phases.

The alteration of lateral intermolecular interactions by cholesterol is well-established from an array of earlier work; however, much less is known regarding how the presence of cholesterol modifies the interactions between membranes. In this work, DPPC membranes with 8 mol % cholesterol were studied to quantify and understand how the addition of cholesterol to a DPPC membrane impacts supported membrane structure and membrane−membrane interactions in the gel phase. A comparison is made between measured membrane interaction force−distance profiles by surface force apparatus (SFA), neutron scattering structural characterization, vesicle zeta potential (ZP), and membrane structure/topology as determined by atomic force microscopy (AFM).

MATERIALS AND METHODS

Chemicals. 1,2-Dihexadecanoyl-*sn*-glycero-3-phosphoethanolamine (DPPE, melting point, T_M = 63 °C), 1,2-dipalmitoyl-*sn*-glycero-3-phosphocholine (DPPC, T_M = 41 °C), and cholesterol (ovine wool, >98%, T_M = 148 °C) were purchased from Avanti Polar Lipids, Inc. (Alabaster, AL) and

Received: December 8, 2014
Revised: January 30, 2015
Published: February 6, 2015

DOI: 10.1021/la504771a
Langmuir 2015, 31, 2527−2532

used as received. 2-(4,4-Difluoro-5,7-diphenyl-4-bora-3*a*,4*a*-diaza-*s*-indacene-3-pentanoyl)-1-hexadecanoyl-*sn*-glycero-3-phosphocholine (*β*-BODIPY 530/550 C_5-HPC) was purchased from Life Technologies (Carlsbad, CA). Electrolyte solutions used $NaNO_3$ (99.995%, Sigma, St. Louis). Water was purified with a Milli-Q gradient water purification system to a resistivity of 18 MΩ·cm.

Sample Preparation. Mica substrate supported lipid bilayers were used in SFA, fluorescence microscopy (FM), and AFM studies. Neutron scattering studies used ultra smooth, single-crystal quartz. The membranes were constructed using Langmuir-Blodgett (LB) deposition (Nima Coventry, U.K.). The inner monolayer for SFA, FM, and AFM experiments was DPPE LB-deposited at 45 mN/m and dipping speed of 1 mm/min. Previous studies show that LB-deposited DPPE forms an almost defect-free, robust, and strongly physisorbed monolayer on mica with transfer ratios of 0.997 ± 0.004[22] with a thickness of 2.56 ± 0.05 nm under these conditions.[23] The tight packing and stability of the gel-phase DPPE inner monolayer minimizes molecular exchange between the two leaflets and provides an ideal base for the 92:8 monolayer, which is the primary interest of this study. In all cases, the outer monolayer was 92:8 DPPC−cholesterol deposited at 30 mN/m. For the SFA, FM, and AFM work, the outer leaflet was LB-deposited with a dipping speed of 4 mm/min. The transfer ratio of the outer monolayer was 0.843 ± 0.057. Mixtures for FM imaging contained 0.5% of BODIPY-HPC. For neutron scattering measurements, a symmetric membrane of 92:8 DPPC−cholesterol was used for the ease of modeling and analysis. The inner leaflet was deposited by LB at 30 mN/m and dipping speed of 1 mm/min on quartz substrates. Because of the weaker adhesion of the membrane to quartz vs mica, the outer leaflet was deposited by the Langmuir−Schaefer (LS) method where the monolayer-coated quartz was stamped horizontally through the lipid monolayer on the air−water interface to form the symmetric bilayer. The isotherm for 92:8 DPPC−cholesterol is shown in Figure 1.

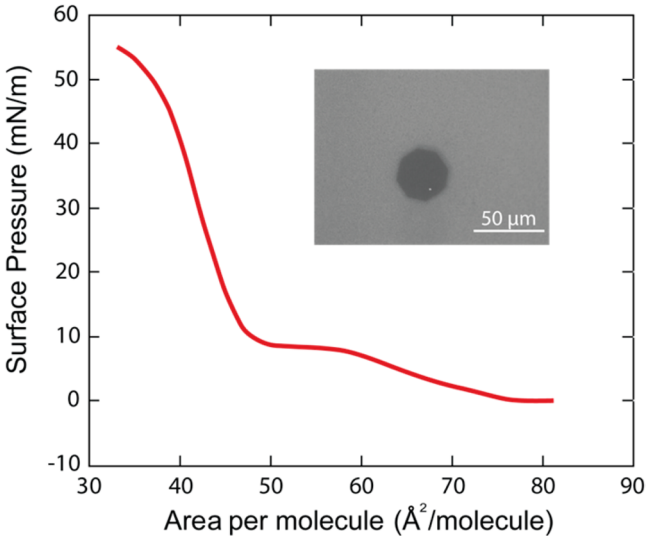

Figure 1. Isotherm of 92:8 DPPC−cholesterol at 25 °C. (Inset) FM image of the 92:8 DPPC−cholesterol membrane at 40× magnification with a photobleached spot. The diffusivity of the DPPC−cholesterol mixtures was very low (almost no recovery observed after 3 h).

Vesicle solutions for zeta-potential measurements were prepared using the extrusion method. 92:8 DPPC−cholesterol mixtures were prepared in chloroform, dried under nitrogen, and then placed under vacuum for at least 4 h. The dried lipids were hydrated with 0.5 mM $NaNO_3$ solution prepared in Milli-Q water to a concentration of 0.4 mg/mL, heated to a temperature of 50 °C, and then extruded through a 100 nm pore size polycarbonate membrane for 10 passes while maintaining the temperature around 50 °C. After the extrusion process, the vesicle solution was placed in a warm water bath (∼50 °C) and then cooled down slowly to 25 °C by placing the bath with the vesicle solution in a temperature-controlled room at 25 °C.

Surface Force Measurements (SFA). The SFA technique has been used extensively to measure the interaction forces between surfaces and details of the technique can be found in the following references.[24−26] On the basis of multiple-beam interferometry, the SFA provides a definitive reference for the surface separation (±0.2 nm in this work). Briefly, one of the membrane-coated mica surfaces was mounted on a fixed stage and the other on a double cantilever spring of known stiffness (∼2.6 × 10^5 mN/m) which can be displaced vertically. The back of the mica substrates was coated with a 55 nm thick, evaporated silver layer. The silver layer on each disk partially transmits light directed normally through the surfaces which constructively interferes, producing fringes of equal chromatic order (FECO). The distances between the surfaces can be measured by observation of the position and displacement of FECO peak wavelengths within a spectrometer. A custom automated SFA Mark-II was used for data collection.[27] The system enables constant and/or variable surface displacements via a computer-controlled motor system. A sensitive CCD camera (Princeton SPEC-10:2K Roper Scientific, Trenton, NJ) was interfaced with the spectrometer and computer acquisition system to allow automated FECO wavelength determination, which was used to determine the separation distance.

After lipid bilayer deposition, the surfaces were transferred and mounted into the SFA under water. The water in the SFA was saturated with 92:8 DPPC−cholesterol to minimize desorption from the surface during the course of the measurements. After the surfaces were mounted, the SFA was placed in a temperature-controlled room at 25.0 °C for at least 2 h to allow equilibration. The membrane thickness was determined using the FECO wavelength shift from membrane contact relative to bare mica substrates after completing each experiment. As the membranes were asymmetric with inner leaflets of DPPE and outer leaflets of DPPC containing 8 mol % cholesterol, we treat the two outer leaflets, which we are primarily interested in, as an equivalent membrane of the mixture composition. Force profiles shown in the results section are from three independent experiments which represent the range of typical force profiles obtained from six completely independent SFA experiments.

Atomic Force Microscopy (AFM). AFM images were acquired using a MFP3D-SA system (Asylum Research, Santa Barbara, CA). A silicon nitrite cantilever (model AC240, Bruker, Santa Barbara, CA) with force constant of 1 N/s was used for imaging. All the images were acquired in contact mode in Milli-Q gradient water with a force of 37 nN. AFM images were analyzed using Gwyddion Version 2.31 (http://gwyddion.net/).

Fluorescence Microscopy (FM). FM images were acquired using a Nikon Eclipse E600 microscope connected

DOI: 10.1021/la504771a
Langmuir 2015, 31, 2527−2532

with CoolSNAP-Pro CCD camera at 10× and 40× magnification.

Zeta-Potential Measurements. ZP was used to quantify the magnitude of the electrical charge based on measurements of vesicle mobility in an electric field in 0.5 mM $NaNO_3$ electrolyte solutions (Brookhaven Zeta Plus, Holtsville, NY). Although not identical with the surface charge or surface potential determination from force profile measurements by SFA, ZP provides the sign of the electrical charge and its relative magnitude referenced between the hydrodynamic shear plane at the vesicle surface and the bulk solution. ZP results were obtained from six independent samples with ten measurements per sample.

Neutron Reflectivity (NR). Reflectivity, R, is defined as the ratio of the number of neutrons elastically and specularly scattered from a surface to that of the incident beam. When measured as a function of wave-vector transfer, $Q_Z = |k_{out} - k_{in}| = (4\pi \sin \theta/\lambda)$, where θ is the angle of incidence and λ is the wavelength of the neutron beam, the reflectivity curve contains information regarding the sample-normal profile of the in-plane averaged scattering length density (SLD) and is therefore most suited for studies of interfacial, layered films. From the measured reflectivity profile, the thickness, SLD, and roughness of the membrane normal to the substrate can be determined by minimizing the difference between the measured reflectivity profile and that obtained from a modeled SLD profile of the membrane.[28]

NR experiments were performed on the SPEAR beamline at the Manuel Lujan Neutron Scattering Center (Los Alamos National Laboratory). Neutron reflectivities down to $R \approx 1 \times 10^{-6}$ and momentum transfers out to $Q_z = \sim 0.2$ Å^{-1} were obtained. The uncertainty of the Q_z resolution, $\sigma Q_z/Q_z$, including instrumental resolution, was approximately 3% for the entire range of scattering vectors. NR data was modeled using Motofit (Rev. 409), a module in IgorPro 6.31. All measurements were done in D_2O at room temperature which varied between 24 and 28 °C, well below the melting point of the membrane. Three independent experiments were done and about the same membrane thickness was obtained from each of the experiments. The NR profile shown in the results section is the data set from the most complete (highest quality) membrane.

RESULTS AND DISCUSSION

Force–Distance Profiles of 92:8 DPPC–Cholesterol Membranes. Figure 2 shows three independently measured force–distance profiles between opposing 92:8 DPPC–cholesterol membranes in 0.5 mM $NaNO_3$. The three different profiles capture the variation in measurements from six independent experiments. The average thickness obtained across all the measurements for an equivalent 92:8 DPPC–cholesterol bilayer was 5.9 ± 0.3 nm.

A weak, long-range electrostatic repulsion was apparent in the force profiles with a decay length consistent with the electrolyte concentration. The electrostatic repulsion was fit using the Poisson–Boltzmann equation yielding a surface charge density of 1.0 ± 0.5 mC/m^2 or surface potential of 19 ± 3 mV with the origin of charge at the membrane surface.[29] Although the ionization constant of cholesterol and phosphatidylcholine lipids[30,31] would suggest an overall neutral charge for the membranes, the presence of charged lipid impurities has been previously reported.[22,32] The measured surface charge density corresponds to 1 negative charge per 400 lipids, or 0.25

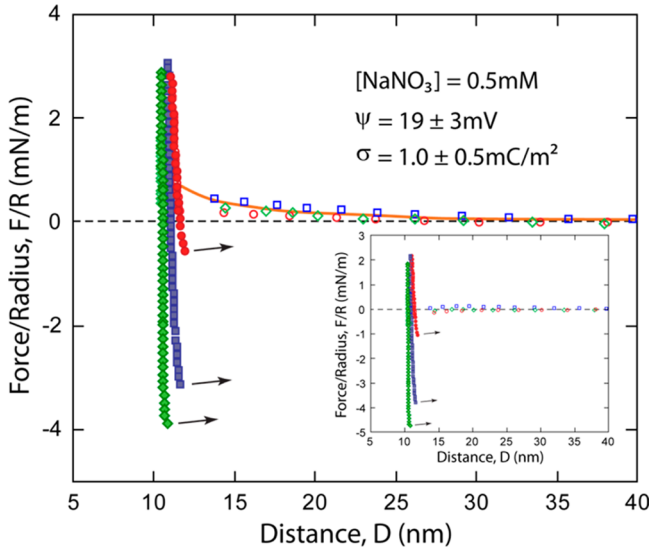

Figure 2. Force–distance profiles between 92:8 DPPC–cholesterol membranes in 0.5 mM $NaNO_3$ solution and fit of the electrostatic contribution (solid line) with the origin of charge at the membrane interface. $D = 0$ is defined as contact between the mica substrates (open symbols, approach; filled symbols, separation). (Inset) The same force profiles after subtracting the electrostatic contribution to quantify the magnitude of the attractive adhesion between the membranes.

mol % of impurities present in the mixture. To corroborate and further quantify the electrostatic repulsion in the 92:8 DPPC–cholesterol system, the zeta potential of vesicle suspensions was measured. The zeta potential of 92:8 DPPC–cholesterol vesicles was −9.8 ± 3.8 mV,[33] which is in good agreement with the electrostatic charge measured in the SFA and our previous zeta potential measurements of similar lipid compositions.[22] The zeta potential and low incidence of membrane spanning defects observed from AFM scans, as described later, are consistent with the source of the electrostatic repulsion being due to the presence of lipid impurities with the origin of charge at the membrane surface.

To better quantify the adhesion between the membranes, the electrostatic repulsion was subtracted from the force profile as shown in the inset of Figure 2. The adhesion between the 92:8 DPPC–cholesterol membranes varied from −1.1 ± 0.1 to −4.7 ± 0.1 mN/m and was reproducible for a given contact region between the membranes. The strength of adhesion at the low end is comparable to pure gel-phase DPPC membranes.[34,35] The higher adhesion values of some membrane contact positions are attributed to hydrophobic attraction due to membrane defects. Specifically, AFM scans of the 92:8 DPPC–cholesterol membrane (Figure 3) revealed nanoscopic monolayer defects in the outer 92:8 monolayer that extend down to the inner DPPE monolayer. The average depth of the defects was 2.5 ± 0.2 nm. The lateral size of the defects was remarkably uniform, diameter of 230 ± 30 nm. AFM scans of cholesterol devoid membranes (a pure DPPC leaflet on an inner DPPE leaflet) showed an order of magnitude fewer defects, strongly suggesting that the incorporation of cholesterol correlates with more defects (see Supporting Information).[36] These defects expose hydrophobic moieties resulting in a commensurate increase in the measured adhesion between the opposing membranes due to hydrophobic attraction. The variability in the adhesion is attributed to inhomogeneities in the membrane

DOI: 10.1021/la504771a
Langmuir 2015, 31, 2527–2532

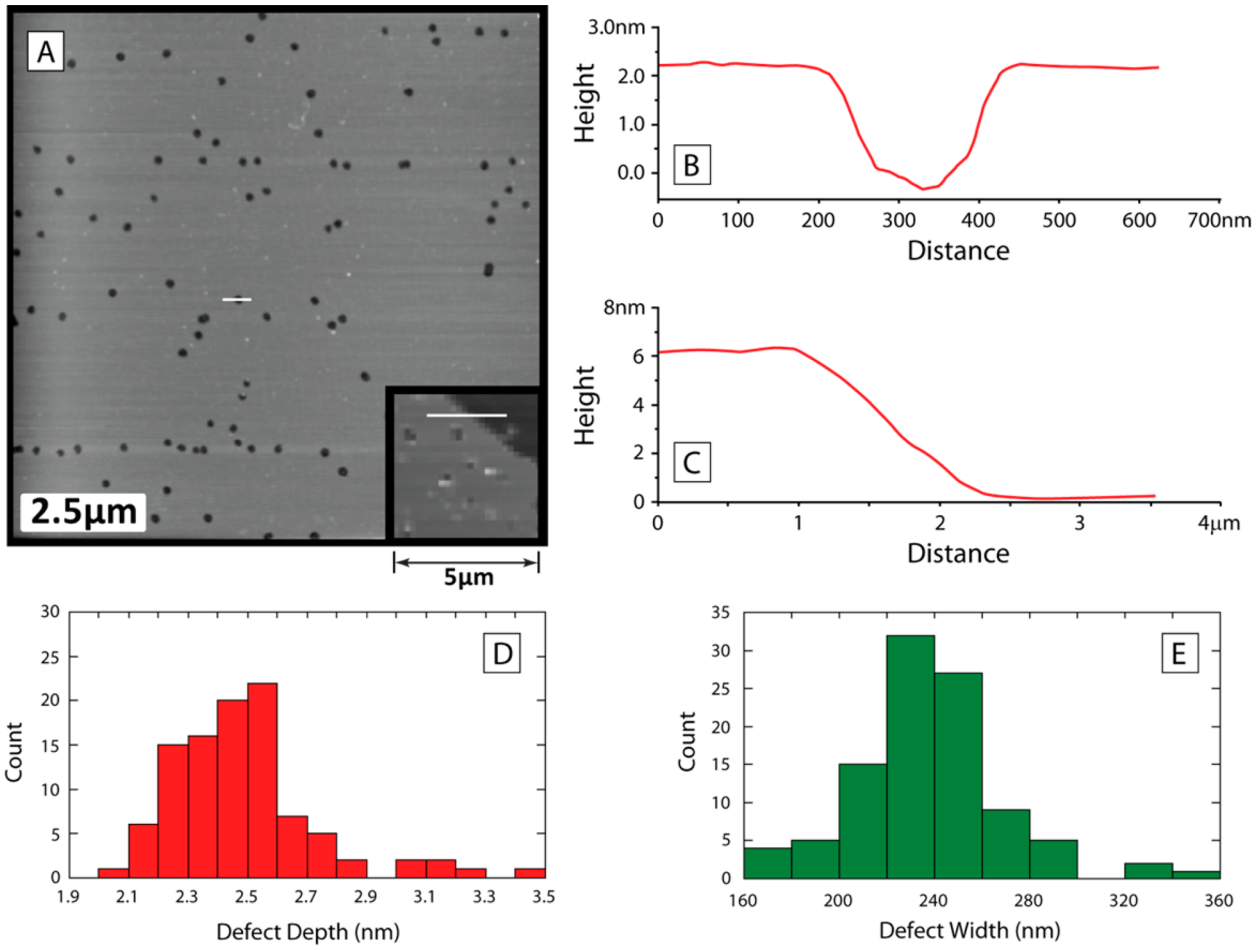

Figure 3. (A) 10 × 10 μm and (inset) 5 μm × 5 μm AFM topography images of the 92:8 DPPC−cholesterol system. (B) and (C) Corresponding cursor profiles as indicated in (A) and inset of image (A) respectively to obtain height profiles. (D) and (E) Histogram of defect depth and width across the sample, respectively.

defect density, which ranged from 1 to 5% surface coverage,[37] rather than structural rearrangements as observed in fluid-phase systems.[22] In one case, a membrane spanning hole that reached the mica substrate was detected by AFM (Figure 3B). The height scan thickness of the membrane was ∼6 nm, which is in good agreement with the membrane thickness obtained from SFA measurements.

In all cases, membrane restructuring or thinning of the membrane was negligible during the course of an experiment, even under increased loads at contact. Reproducible force profiles and adhesive minima for a given contact position strongly suggests that the system does not rearrange during the time scale of the experiment. This observed trend is consistent with the small size of the defects and the gel-phase behavior of the membrane (see Figure 1). Further, hemifusion was not observed in any of the experiments due to the low diffusion and relatively low applied force during the course of the experiments. Conversely, fluid-phase membranes containing defects have been shown to restructure in contact, resulting in adhesion that depends on the applied load and contact time of the opposing membranes.[22]

Neutron Scattering Studies. The structure of supported 92:8 DPPC−cholesterol membranes on quartz was also characterized using NR and Figure 4 shows the best data set from three independent experiments. The thickness of the membrane was consistent between the three measurements,

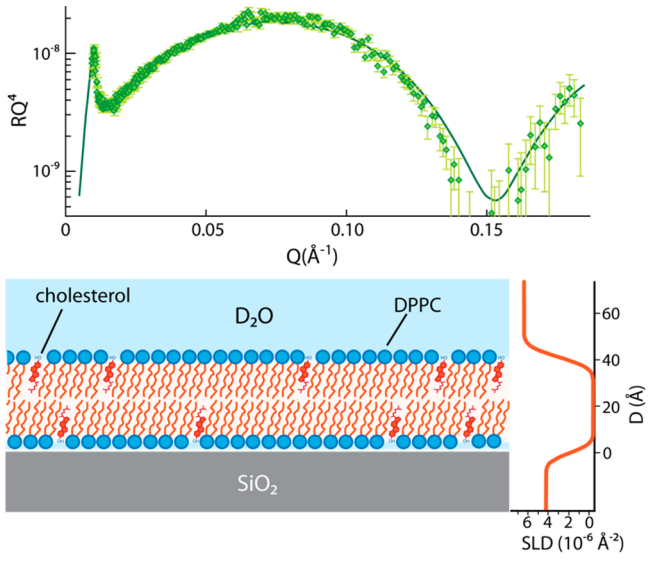

Figure 4. (Top image) Fit of RQ^4 vs Q from the neutron reflectivity data. (Bottom image) Schematic of the supported membrane and corresponding neutron scattering length density profile of the membrane obtained from fitting the data.

but the SLD of the hydrocarbon region was somewhat higher for the other two cases. The hydrocarbon region SLD is

DOI: 10.1021/la504771a
Langmuir 2015, 31, 2527−2532

indicative of membrane defects as the presence of D_2O in the defects increases the SLD. Because of the resolution of the NR data, which was primarily sensitive to the hydrocarbon region (acyl chains) of the bilayer, a simple one-layer model of the membrane was used to represent the hydrocarbon region and fit the data. The thickness of the box was 4.15 ± 0.10 nm with an SLD of $-0.3 \pm 0.2 \times 10^{-6}$ Å^{-2}. This value is in excellent agreement with the SLD of pure gel-phase PC hydrocarbon tails of -0.41×10^{-6} Å^{-2} by Fragneto et al.[38] given that the neutron SLD of cholesterol is 0.21×10^{-6} Å^{-2} and a defect density less than 5%.[39,40] The other samples had somewhat higher hydrocarbon region SLDs, indicative of higher defect densities. The uniform thickness of the hydrocarbon region for all the samples is also consistent with nanoscopic rather than macroscopic defects.

CONCLUSIONS

As one of the major components in biological membranes, the functions and properties of cholesterol have been widely studied and documented. In this work, a simplified system of a substrate-supported membrane was used to measure the interaction forces between two cholesterol-containing membranes and the structure of the membranes with ultrahigh resolution. The interaction force−distance profiles between DPPC−cholesterol membranes measured using SFA and AFM imaging of the membrane revealed the presence of nanoscopic defects, leading to an enhanced hydrophobic attraction between the membranes in contact. The nonhomogeneity in the lateral defect distribution across the membrane, as demonstrated by AFM and neutron scattering studies, leads to variation in the thickness of the membrane and membrane−membrane adhesion. A weak electrostatic repulsion due to the presence of charged lipid impurities was detected and further quantified by vesicle zeta potential measurements. Such studies demonstrate that cholesterol alters the intersurface interaction and membrane structure in complex and important ways.

ASSOCIATED CONTENT

Supporting Information

Comparison of atomic force microscopy (AFM) images of DPPC and 92:8 DPPC−cholesterol membrane. This material is available free of charge via the Internet at http://pubs.acs.org.

AUTHOR INFORMATION

Corresponding Author

*E-mail: tlkuhl@ucdavis.edu.

Notes

The authors declare no competing financial interest.

ACKNOWLEDGMENTS

This work was primarily supported by the NSF chemistry division through Grant CHE-0957868 and completed under CHE-1413745. This work benefited from the neutron research facilities of the Manual Lujan Jr. Neutron Scattering Center which is supported by DOE under Contract No. W7405-ENG-36. We thank Joao Ventrici for assistance with atomic force microscopy, Araceli Munaier Almeida for assistance with transfer ratio measurements, and Christy Michelle Turcios for assistance with fluorescence microscopy measurements.

REFERENCES

(1) Drolle, E.; Kucerka, N.; Hoopes, M. I.; Choi, Y.; Katsaras, J.; Karttunen, M.; Leonenko, Z. Effect of melatonin and cholesterol on the structure of DOPC and DPPC membranes. *Bba-Biomembranes* **2013**, *1828* (9), 2247−2254.

(2) Rawicz, W.; Smith, B. A.; McIntosh, T. J.; Simon, S. A.; Evans, E. Elasticity, strength, and water permeability of bilayers that contain raft microdomain-forming lipids. *Biophys. J.* **2008**, *94* (12), 4725−4736.

(3) Jurak, M. Thermodynamic Aspects of Cholesterol Effect on Properties of Phospholipid Monolayers: Langmuir and Langmuir-Blodgett Monolayer Study. *J. Phys. Chem. B* **2013**, *117* (13), 3496−3502.

(4) Almeida, P. F. F. Thermodynamics of lipid interactions in complex bilayers. *Bba-Biomembranes* **2009**, *1788* (1), 72−85.

(5) Needham, D.; Nunn, R. S. Elastic-Deformation and Failure of Lipid Bilayer-Membranes Containing Cholesterol. *Biophys. J.* **1990**, *58* (4), 997−1009.

(6) Dietrich, C.; Bagatolli, L. A.; Volovyk, Z. N.; Thompson, N. L.; Levi, M.; Jacobson, K.; Gratton, E. Lipid rafts reconstituted in model membranes. *Biophys. J.* **2001**, *80* (3), 1417−1428.

(7) Silvius, J. R. Role of cholesterol in lipid raft formation: lessons from lipid model systems. *Bba-Biomembranes* **2003**, *1610* (2), 174−183.

(8) Crane, J. M.; Tamm, L. K. Role of cholesterol in the formation and nature of lipid rafts in planar and spherical model membranes. *Biophys. J.* **2004**, *86* (5), 2965−2979.

(9) Cinek, T.; Horejsi, V. The Nature of Large Noncovalent Complexes Containing Glycosyl-Phosphatidylinositol-Anchored Membrane-Glycoproteins and Protein Tyrosine Kinases. *J. Immunol.* **1992**, *149* (7), 2262−2270.

(10) Ahmed, S. N.; Brown, D. A.; London, E. On the origin of sphingolipid/cholesterol-rich detergent-insoluble cell membranes: Physiological concentrations of cholesterol and sphingolipid induce formation of a detergent-insoluble, liquid-ordered lipid phase in model membranes. *Biochemistry* **1997**, *36* (36), 10944−10953.

(11) Smaby, J. M.; Brockman, H. L.; Brown, R. E. Cholesterols Interfacial Interactions with Sphingomyelins and Phosphatidylcholines - Hydrocarbon Chain Structure Determines the Magnitude of Condensation. *Biochemistry* **1994**, *33* (31), 9135−9142.

(12) Wydro, P.; Knapczyk, S.; Lapczynska, M. Variations in the Condensing Effect of Cholesterol on Saturated versus Unsaturated Phosphatidylcholines at Low and High Sterol Concentration. *Langmuir* **2011**, *27* (9), 5433−5444.

(13) Fliesler, S. J.; Schroepfer, G. J. Sterol Composition of Bovine Retinal Rod Outer Segment Membranes and Whole Retinas. *Biochim. Biophys. Acta* **1982**, *711* (1), 138−148.

(14) Bloch, K. Cholesterol: evolution of structure and function. In *Biochemistry of lipids, lipoproteins, and membranes*; Vance, D. E., Vance, J. E., Eds.; Elsevier: Amsterdam, 1991; pp 363−381.

(15) Anderson, T. G.; McConnell, H. M. Condensed complexes and the calorimetry of cholesterol-phospholipid bilayers. *Biophys. J.* **2001**, *81* (5), 2774−2785.

(16) Brown, D. A.; London, E. Structure and function of sphingolipid- and cholesterol-rich membrane rafts. *J. Biol. Chem.* **2000**, *275* (23), 17221−17224.

(17) Yuan, C.; Johnston, L. J. Phase evolution in cholesterol/DPPC monolayers: atomic force microscopy and near field scanning optical microscopy studies. *J. Microsc. (Oxford, U.K.)* **2002**, *205*, 136−146.

(18) Marsh, D. Cholesterol-induced fluid membrane domains: A compendium of lipid-raft ternary phase diagrams. *Bba-Biomembranes* **2009**, *1788* (10), 2114−2123.

(19) Marsh, D. Liquid-ordered phases induced by cholesterol: A compendium of binary phase diagrams. *Bba-Biomembranes* **2010**, *1798* (3), 688−699.

(20) Stottrup, B. L.; Keller, S. L. Phase behavior of lipid monolayers containing DPPC and cholesterol analogs. *Biophys. J.* **2006**, *90* (9), 3176−3183.

(21) Mills, T. T.; Huang, J. Y.; Feigenson, G. W.; Nagle, J. F. Effects of cholesterol and unsaturated DOPC lipid on chain packing of

DOI: 10.1021/la504771a
Langmuir 2015, 31, 2527−2532

saturated gel-phase DPPC bilayers. *Gen. Physiol. Biophys.* **2009**, *28* (2), 126−139.
(22) Kurniawan, J.; Yin, N. N.; Liu, G. Y.; Kuhl, T. L. Interaction Forces between Ternary Lipid Bilayers Containing Cholesterol. *Langmuir* **2014**, *30* (17), 4997−5004.
(23) Kienle, D. F.; de Souza, J. V.; Watkins, E. B.; Kuhl, T. L. Thickness and refractive index of DPPC and DPPE monolayers by multiple-beam interferometry. *Anal. Bioanal. Chem.* **2014**, *406* (19), 4725−4733.
(24) Israelachvili, J. N.; Adams, G. E. Measurement of Forces between Two Mica Surfaces in Aqueous-Electrolyte Solutions in Range 0-100 nm. *J. Chem. Soc., Faraday Trans. 1* **1978**, *74*, 975−1001.
(25) Israelachvili, J. N. Thin-Film Studies Using Multiple-Beam Interferometry. *J. Colloid Interface Sci.* **1973**, *44* (2), 259−272.
(26) Kuhl, T. L.; Leckband, D. E.; Lasic, D. D.; Israelachvili, J. N. Modulation of Interaction Forces between Bilayers Exposing Short-Chained Ethylene-Oxide Headgroups. *Biophys. J.* **1994**, *66* (5), 1479−1488.
(27) Moore, N. W.; Mulder, D. J.; Kuhl, T. L. Adhesion from tethered ligand-receptor bonds with microsecond lifetimes. *Langmuir* **2008**, *24* (4), 1212−1218.
(28) Kjaer, K. Some Simple Ideas on X-Ray Reflection and Grazing-Incidence Diffraction from Thin Surfactant Films. *Physica B* **1994**, *198* (1−3), 100−109.
(29) Grabbe, A.; Horn, R. G. Double-Layer and Hydration Forces Measured between Silica Sheets Subjected to Various Surface Treatments. *J. Colloid Interface Sci.* **1993**, *157* (2), 375−383.
(30) Tsui, F. C.; Ojcius, D. M.; Hubbell, W. L. The Intrinsic Pka Values for Phosphatidylserine and Phosphatidylethanolamine in Phosphatidylcholine Host Bilayers. *Biophys. J.* **1986**, *49* (2), 459−468.
(31) Moncelli, M. R.; Becucci, L.; Guidelli, R. The Intrinsic Pk(a), Values for Phosphatidylcholine, Phosphatidylethanolamine, and Phosphatidylserine in Monolayers Deposited on Mercury-Electrodes. *Biophys. J.* **1994**, *66* (6), 1969−1980.
(32) Pincet, F.; Cribier, S.; Perez, E. Bilayers of neutral lipids bear a small but significant charge. *Eur. Phys. J. B* **1999**, *11* (1), 127−130.
(33) A positive shift in the measured ZP value was observed over time in some of the measurements. Typically, such shifts are associated with changes in the vesicle suspension with the application of an electric field, consistent with gel-phase vesicle instability and fusion. Therefore, the reported value of Ψ for the 92:8 DPPC−cholesterol vesicles was the average of all measurements before the positive shift was observed.
(34) Marra, J.; Israelachvili, J. Direct Measurements of Forces between Phosphatidylcholine and Phosphatidylethanolamine Bilayers in Aqueous-Electrolyte Solutions. *Biochemistry* **1985**, *24* (17), 4608−4618.
(35) Orozco-Alcaraz, R.; Kuhl, T. L. Interaction Forces between DPPC Bilayers on Glass. *Langmuir* **2013**, *29* (1), 337−343.
(36) Our measurements of six DPPC on the DPPE system were consistent with earlier studies by Marra and Israelachvili yielding an adhesion of -0.9 ± 0.2 mN/m.
(37) The defect density was calculated from more than 60 10×10 μm AFM scans. The analysis scan size was chosen to be about the same size as the membrane contact region in the SFA experiments.
(38) Fragneto, G.; Graner, F.; Charitat, T.; Dubos, P.; Bellet-Amalric, E. Interaction of the third helix of Antennapedia homeodomain with a deposited phospholipid bilayer: A neutron reflectivity structural study. *Langmuir* **2000**, *16* (10), 4581−4588.
(39) Greenwood, A. I.; Tristram-Nagle, S.; Nagle, J. F. Partial molecular volumes of lipids and cholesterol. *Chem. Phys. Lipids* **2006**, *143* (1−2), 1−10.
(40) The SLD of cholesterol was calculated using the partial molar volume of cholesterol embedded in a DPPC membrane assuming that cholesterol was oriented normal to the bilayer plane. The subphase D_2O has large SLD contrast to the acyl chain of lipids which enable us to quantify the defect density. The SLD of the hydrocarbon region indicates a complete bilayer was deposited with less than 5% defects.

DOI: 10.1021/la504771a
Langmuir 2015, 31, 2527−2532